Magnetic Droplet Mode in a Vertical Nanocontact-Based Spin Hall Nano-Oscillator at Oblique Fields

Lina Chen,[1,2] S. Urazhdin,[3] Kaiyuan Zhou,[1,2] Y.W. Du,[1] and R.H. Liu[1,2,3,*]

[1] *National Laboratory of Solid State Microstructures, School of Physics and Collaborative Innovation, Center of Advanced Microstructures, Nanjing University, Nanjing, 210093, China*

[2] *Shenzhen Research Institute of Nanjing University, Shenzhen, 570126, China*

[3] *Department of Physics, Emory University, Atlanta, Georgia 30322, USA*

(Received 16 September 2019; revised manuscript received 25 November 2019; accepted 24 January 2020; published 13 February 2020)

We experimentally demonstrate an alternative type of spin Hall nano-oscillator based on a vertical nanocontact fabricated on a Pt/(Co/Ni) multilayer. We analyze the spectral characteristics of the nano-oscillator as a function of current, magnetic field, and temperature. At sufficiently large currents, the oscillator exhibits dynamics at a frequency far below the ferromagnetic resonance, which at large fields exhibits a redshift with increasing current. At smaller fields and low temperatures, the frequency becomes nearly independent of current, with a well-defined threshold current. These distinct spectral characteristics of the demonstrated nano-oscillator can be explained by the formation of the magnetic droplet—a dissipative magnetic soliton stabilized by the local injection of spin current produced by the spin Hall effect in Pt. The minimum linewidth exhibits a linear temperature dependence, suggesting single-mode dynamics, and enabling coherent magnetization auto-oscillation at room temperature. The demonstrated nano-oscillator geometry provides alternative opportunities for the development of active nanomagnetic devices and for optimization of their spectral characteristics for applications in microwave technology and spin-wave logic.

DOI: 10.1103/PhysRevApplied.13.024034

I. INTRODUCTION

Spintronics emerged in the 1980s following the discoveries of giant-magnetoresistance and tunneling-magnetoresistance effects in magnetic heterostructures, and experienced a dramatic resurgence in the last 20 years following the discovery of the spin-current-driven spin-torque (ST) effect enabling electronic control of nanomagnetic systems [1,2]. ST can compensate the dynamical damping in magnetic systems, resulting in the excitation of coherent dynamical magnetization states or changes of static magnetic configuration [3]. Intense ongoing efforts are dedicated to exploring the relationship among the nature and the coherence of the dynamical states in magnetic nano-oscillators driven by ST, the magnetic properties, the layout of magnetic nanostructures, and the geometry of spin-current injection [4,5], with the goal of achieving active nanodevice characteristics optimized for applications in radio-frequency electronics, magnonics, and neuromorphic computing. Early efforts focused on the development of ST-driven nano-oscillators (STNOs) used point nanocontacts on extended magnetic multilayers (NC STNOs), which provided a useful platform for the local generation of propagating spin waves in extended active magnetic layers [6–8]. A recently developed alternative platform uses current-induced spin-orbit torques in bilayers of ferromagnets with heavy nonmagnetic metals [9,10], topological insulators [11], or other materials with strong spin-orbit interaction [12]. Among the advantages of this approach are the unprecedented geometric flexibility and the possibility to achieve high efficiency by using spin-orbit materials with a large spin Hall angle [10,11]. Since the spin Hall effect (SHE) usually dominates spin-orbit torque in these ferromagnet/nonmagnetic metal (F/N) systems, they are commonly referred to as "spin Hall nano-oscillators" (SHNOs) [13,14].

The SHNO geometry most-extensively studied to date, because of its simplicity and reproducibility, uses electric current locally injected into an extended F/N bilayer via two sharp closely spaced nonmagnetic electrodes, forming an in-plane nano-contact [13–17]. This geometry is commonly referred to as a "nanogap SHNO." However, studies have shown that the spin-injection geometry in the planar-nanogap SHNO favors simultaneous excitation of two dynamical modes [14,18], resulting in significant degradation of oscillation characteristics at ambient temperatures,

*rhliu@nju.edu.cn

due to the thermal-magnon-mediated mode hopping [19]. In in-plane magnetized nanogap SHNOs, the secondary mode is stabilized mostly by the dipolar field of the primary bullet mode, which creates two effective potential wells in the regions localized near the edges of the center bullet mode along the axis defined by the direction of magnetization [18,20]. The secondary mode localized in these potential wells does not significantly spatially overlap with the primary mode, enabling dynamics at two unrelated frequencies. Multimodal dynamics is also commonly observed in an alternative SHNO configuration based on a F/N nanowire [21], due to the small frequency separation among the dynamical modes in a relatively large magnetic system. Meanwhile, SHNO layouts based on bow-tie-shaped nanoconstrictions in extended F/N bilayers [22] or tapered nanowires [23–25] suffer from strong mode localization by the dipolar edge fields, diminishing their thermal stability. The same dipolar effects also make it challenging to use such layouts for the generation of propagating pin waves in magnonic circuits. These limitations of the existing SHNO geometries underscore the need to explore alternative geometries and device-operation regimes.

Here we experimentally demonstrate a SHNO based on a vertical nanocontact (VNC) fabricated on an extended Pt/(Co/Ni) bilayer [26]. At small currents, modest out-of-plane fields, and cryogenic temperatures, the VNC SHNO developed exhibits a low-intensity, high-frequency spectral peak, and frequency redshift with increasing current, as expected for the nonlinear self-localized bullet mode commonly observed in SHNOs [13–15] and STNOs with in-plane magnetization [27]. At increased temperatures, the bullet mode rapidly broadens and disappears, also similar to the behaviors commonly observed for the planar-nanogap SHNOs. However, at larger currents and small fields, the oscillator exhibits an abrupt onset of an intense low-frequency mode above a certain well-defined threshold current I_{th}, which rapidly decreases with increasing applied magnetic field. The oscillation frequency of this mode is nearly independent of the current. On the basis of our observations, we identify this mode as a magnetic droplet—a localized standing dissipative soliton nucleated and stabilized by the local injection of spin current. In contrast to the exponential temperature dependence of the linewidth of the bullet mode in a nanogap SHNO with in-plane magnetization, our VNC SHNO exhibits a linear temperature dependence of the linewidth, consistent with thermal broadening of single-mode oscillation, resulting in higher thermal stability and a small minimum linewidth of 4.5 MHz at room temperature. Single-mode dynamics is facilitated by the geometry of the droplet, which consists of an inverted core surrounded by a region experiencing large-amplitude precession. In contrast to the bullet mode, in this geometry the effective dipolar potential well, produced by the fringe field of the inverted core, is colocalized with the precessing region, thus preventing the formation of a secondary mode. Our findings indicate that the demonstrated VNC SHNO provides a viable route for achieving spin-Hall-effect-driven coherent single-mode dynamical states at room temperature.

II. DEVICE FABRICATION AND ELECTRONIC CHARACTERISTICS

Our device geometry and experimental setup are schematically shown in Fig. 1(a). The device is based on a Pt(10 nm)/$[$Co(0.2 nm)/Ni(0.3 nm)$]_{10}$ magnetic multilayer deposited on an annealed sapphire substrate by sputtering at room temperature. Magnetic characterization [28] shows that the magnetic film exhibits interfacial perpendicular magnetic anisotropy (PMA) of approximately 3.6 kOe, which is smaller than the demagnetizing field of approximately 7.0 kOe, resulting in a modest net in-plane anisotropy. As a result, we expect that the film becomes obliquely magnetized at the relatively large nearly normal fields applied in our measurements [28]. Additionally, because of the scale dependence of the dipolar effects, these Co/Ni multilayer films are also expected to support nanoscale vortexlike or magnetic domain structures under a certain range of out-of-plane magnetic fields [29]. Therefore, in the following we refer to the studied magnetic system as exhibiting PMA. The nanocontact structure, fabricated by multistep electron-beam lithography, consists of a 4-μm-wide, 10-μm-long Pt/(Co/Ni) multilayer strip with an approximately-100-nm circular Au nanocontact on top and two micrometer-scale Au electrodes attached to the Au nanocontact and to the edge of the multilayer strip. The electrodes are electrically insulated by a 100-nm-thick cross-linked insulating polymer (PMMA).

We now briefly discuss the characteristics of the VNC SHNO expected on the basis of its geometry. The current distribution and the resulting Oersted field are numerically calculated with COMSOL MULTIPHYSICS [30] with a resistivity of 20 $\mu\Omega$ cm for the (Co/Ni)(5 nm) layer, 14 $\mu\Omega$ cm for the Pt(10 nm) layer, and 1.7 $\mu\Omega$ cm for the Au electrodes. Because of the radial current flow in the bottom electrode formed by the Pt/(Co/Ni) multilayer, the current density in Pt reaches its largest values near the edges of the nanocontact [Fig. 1(b)]. The current generates a chiral Oersted field in the Co/Ni multilayer, which is also the largest close to the edges of the nanocontact [Fig. 1(c)]. COMSOL MULTIPHYSICS simulations show that the out-of-plane component of the Oersted field contributes less than approximately 5% to the total Oersted field in the vicinity of the nanocontact. Thus, only the in-plane component of Oersted field $H_{\text{in-Oe}}$ is taken into account in the micromagnetic simulations discussed below. Additionally, the current-induced spin Hall effect in Pt produces a local spin current injected into the Co/Ni multilayer [Fig. 1(d)]. Figure 1(e) shows a section through the center of the device of the calculated distribution of the current density $J_c(y)$

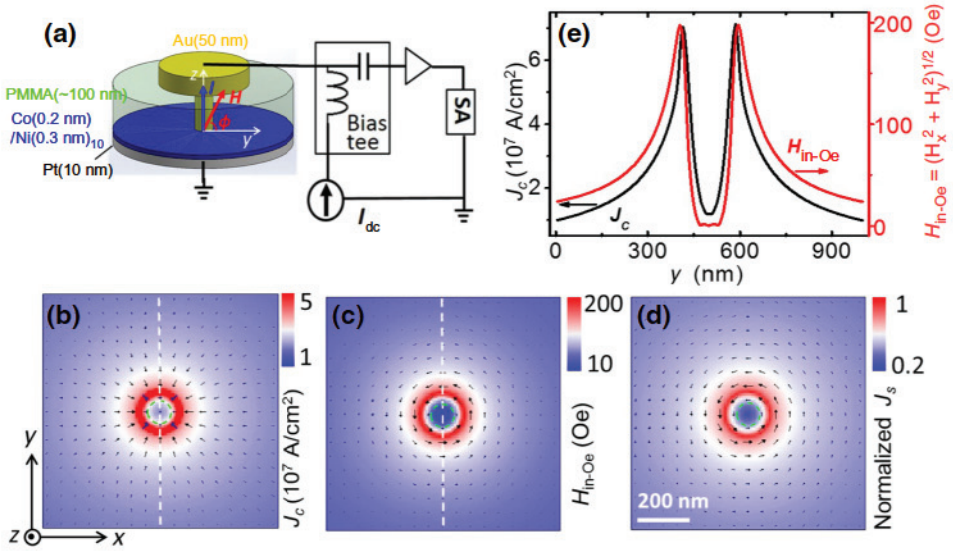

FIG. 1. Structure and electronic characteristics of the VNC SHNO based on a Pt/(Co/Ni) bilayer. (a) The device structure and the experimental setup including dc current source, bias tee, microwave amplifier, and spectrum analyzer (SA). (b)–(d) Color maps of the current distribution in the Pt layer (b), the in-plane Oersted field in the Co/Ni layer (c), and the spin current injected from Pt into Co/Ni (d) calculated with COMSOL MULTIPHYSICS. The scales are indicated to the right of the corresponding plots. The dotted circle marks the nanocontact, and arrows show the directions of the corresponding vector quantities. (e) Calculated magnitude of the current density and the in-plane Oersted field at current $I = 14$ mA along the section shown by the dashed lines in (b),(c).

in Pt, together with the distribution of the in-plane Oersted field $H_{\text{in-Oe}}$ in Co/Ni. These results indicate that both $H_{\text{in-Oe}}$ and J_c (and consequently J_s related to J_c by the spin Hall angle θ_{SH}) decrease by about a factor of 2 within a distance of about 100 nm from the nanocontact edge. The strong localization of spin-current injection results in efficient excitation of local magnetization dynamics, as discussed below. Several features distinguish this geometry from the previously studied SHNO. For instance, the previously studied SHNO used a quasiuniform spin-current polarization, but our VNC SHNO has a chiral spin-current polarization [see Fig. 1(d)], averaging out to zero over the device area.

III. EXPERIMENT

A. Spectral characteristics of the VNC SHNO at 295 K

To experimentally explore the dynamical states induced by spin current in the VNC SHNO structure, we perform spectroscopic measurements with the magnetic field H tilted by angle $\varphi = 82°$ relative to the film plane [Fig. 1(a)]. Tilting of the field enables electrical detection of the oscillating magnetization based on the anisotropic magnetoresistance effect in the Co/Ni multilayer. Figure 2(a) shows representative auto-oscillation spectra acquired at $I = 14$ mA with field H ranging from 800 to 1200 Oe. Additional measurements show that dynamical states can also be excited by negative currents, consistent with the chiral symmetry of the spin-current polarization in the structure studied [see Fig. 1(d)]. The power spectral density (PSD) of the spectra can be well approximated by a Lorentzian function, as shown by the curves in Fig. 2(a), indicating that single-mode dynamics is achieved even at room temperature. To establish the nature of the observed dynamical mode, we analyze its relation to the ferromagnetic resonance (FMR) frequency f_{FMR} of the Co/Ni layer, which is measured by the ST-FMR technique [31]. Figure 2(b) shows the field dependence of f_{FMR}, together with the auto-oscillation frequency f_c obtained at

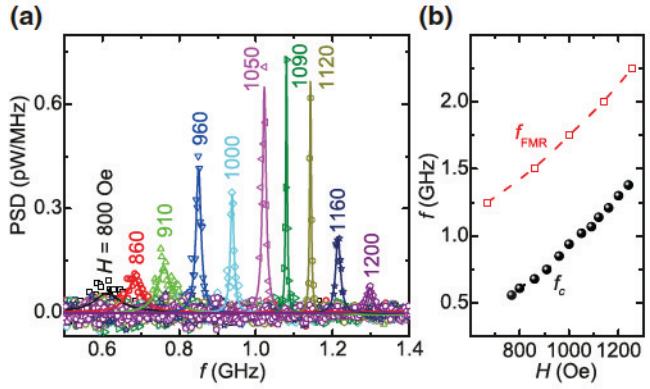

FIG. 2. (a) Microwave-generation spectra (symbols) obtained at $I = 14$ mA, $T = 295$ K, and the labeled values of the magnetic field H. The curves are the results of fitting with the Lorentzian function. (b) Auto-oscillation frequency f_c (solid circles) and the FMR frequency f_{FMR} (squares) versus field H. f_{FMR} is measured by the ST-FMR technique.

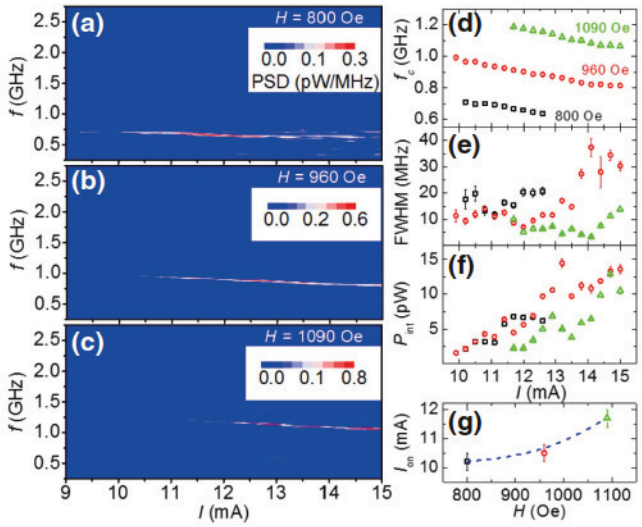

FIG. 3. Dependence of the microwave-generation characteristics on current at $T = 295$ K. (a)–(c). Pseudocolor plots of the spectra obtained at I varied between 9 and 15 mA in 0.3-mA steps at fields $H = 800$ Oe (a), $H = 960$ Oe (b), and $H = 1090$ Oe (c). (d)–(f) Dependence of the central generation frequency f_c (d), FWHM (e), and integral intensity P_{int} (f) on current at $H = 800$ Oe (squares), $H = 960$ Oe (circles), and $H = 1090$ Oe (triangles). f_c, the FWHM, and P_{int} are determined by fitting the power spectra with the Lorentzian function. (g) Dependence of the auto-oscillation-onset current I_{on} of the SHNO on the external field H.

$I = 14$ mA. These data show that f_c is far below f_{FMR}, indicating that the auto-oscillation forms a localized mode.

To obtain further insight into the nature of the dynamical states in the VNC SHNO, we analyze the dependence of the spectral characteristics on the excitation current I at different magnetic fields (Fig. 3). The frequency of auto-oscillation exhibits a small, almost linear, decrease with increasing current for all three values of the field in Fig. 3, while the integral power monotonically increases with current. Meanwhile, the linewidth exhibits a nonmonotonic dependence on current, reaching a minimum FWHM of approximately 4.5 MHz at $I \simeq 13.5$ mA and $H = 1090$ Oe. This value is much smaller than the minimum linewidth of approximately 40 MHz observed at room temperature for planar-nanogap SHNOs based on a Pt/permalloy bilayer with in-plane magnetization and a nanopatterned spin injector [22]. The dependence of the spectral characteristics on the excitation current is similar to that observed in multilayer NC STNOs with out-of-plane magnetized Co/Ni free magnetic layers [32].

We now discuss the relation between the behaviors of the VNC SHNO and other magnetic nano-oscillators, and the implications for the nature of the dynamical mode in our VNC SHNO. Since the oscillation frequency f_c is below the spectrum of propagating spin-wave modes, the dynamical mode must be localized. The localization cannot be attributed entirely to the effects of the Oersted field, because the direction of this field is almost in the plane, while the static magnetization and the external field are both out of the plane. Furthermore, the magnitude of the Oersted field [see Fig. 1(c)] is too small to account for the large frequency difference between the auto-oscillation and the FMR mode [Fig. 2(b)]. Thus, the localization is likely caused by the effect of injected spin current, resulting in the formation of a nonlinearly localized soliton. This conclusion is supported by the calculation results presented in Figs. 1(c) and 1(d).

Prior theoretical calculations and experiments identified two different types of localized dynamical solitonic modes stabilized in magnetic nano-oscillators by spin torque: the spin-wave bullet and the droplet modes [13–15,27,33–36]. The magnetic droplet is a dissipative solitonic mode that consists of a static central core with the magnetization direction opposite the surrounding magnetic film, separated from the latter by a region where the magnetization experiences large-amplitude dynamics. This dynamics is driven by the current-induced spin torque, which together with the magnetic anisotropy also stabilizes the inverted core. The possibility to stabilize the magnetic droplet by the spin current was proposed theoretically [35] and confirmed experimentally for a conventional multilayer STNO with in-plane magnetization of the spin-polarizing layer and PMA of the free magnetic layer at large fields normal to the film plane [33,34]. It was also suggested that a nanoscale magnetic bubble can become trapped in the region of a nonsaturated magnetic film with PMA subjected to local spin-current injection, resulting in the dynamical bubble mode with spatial and spectral characteristics similar to those of the droplet mode [15].

Another localized solitonic mode, termed the "spin-wave bullet," is a nonpropagating spin-wave mode self-localized due to the dynamical magnetic nonlinearity. In contrast to the droplet, the bullet mode is characterized by large-amplitude precession of the central region, with the spatial characteristics determined by a combination of exchange stiffness, nonlinearity, and spin torque [27]. This mode is commonly observed in SHNOs and conventional multilayer STNOs with in-plane magnetic anisotropy, or a PMA free layer at sufficiently large in-plane fields [13,15,19,36]. The magnetic droplet mode is generally expected to exhibit larger spectral intensities than the bullet mode, due to the large precession angle of magnetization in the dynamical domain wall. Furthermore, the frequency of the droplet mode is generally expected to fall far below f_{FMR}, because the dynamics is driven by small torques associated with the unstable domain-wall configuration. In contrast, the dynamics of the bullet mode is driven by the much-larger direct effects of exchange interaction, and its frequency is generally only slightly below f_{FMR} due to the nonlinear dipolar effects associated

with large-amplitude precession [13,27,36]. On the basis of these distinct characteristics, we tentatively conclude that the dynamical mode observed in the VNC SHNO is a dissipative droplet soliton. We provide further evidence for this conclusion below.

B. Spectral characteristics of the VNC SHNO at 60 K

Prior experimental and theoretical studies showed that the bullet mode emerges from the linear spectrum of spin waves above a critical current determined by damping, without any energy barrier for its formation [13,14,19]. In contrast, the droplet mode involves an inverted static core, whose nucleation is associated with a certain energy barrier. This barrier is likely too small to affect the dynamics at room temperature, but its effects can become pronounced at lower temperatures [19,37,38]. To investigate these effects, we perform additional spectroscopic measurements at cryogenic temperatures. Figure 4 shows the microwave-generation spectra acquired at the experimental temperature $T = 60$ K at

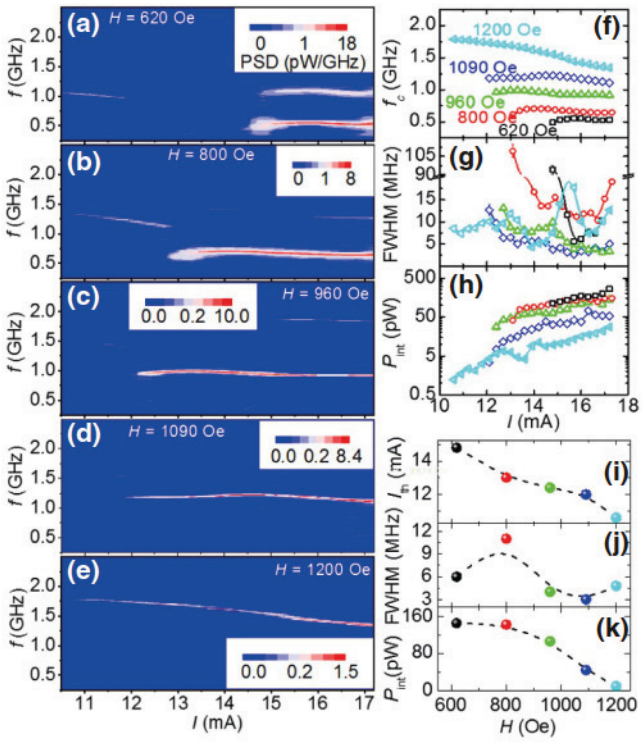

FIG. 4. Dependence of the microwave-generation characteristics on current at $T = 60$ K. (a)–(e) Pseudocolor plots of the spectra obtained at I varied between 10.6 and 17.2 mA in 0.3-mA steps and fields $H = 620$ Oe (a), $H = 800$ Oe (b), $H = 960$ Oe (c), $H = 1090$ Oe (d), and $H = 1200$ Oe (e). (f)–(h) The center frequency f_c (f), FWHM (g), and integral intensity $P_{\rm int}$ (h) of the low-frequency mode m_l versus I extracted from the spectra in (a)–(e) at the labeled fields. (i)–(k) Field dependence of the threshold current $I_{\rm th}$ (i), the minimum FWHM (j), and $P_{\rm int}$(k) of mode m_l obtained at the current I_p defined in the main text.

fields ranging between 620 and 1200 Oe. The actual temperature of the active device area is expected to reach 120 K at current $I = 14$ mA, as estimated from the COMSOL MULTIPHYSICS simulation of Joule heating [30]. In contrast to the room-temperature spectra, which exhibit only a single low-frequency mode m_l at sufficiently high currents, the cryogenic temperature spectra reveal a low-intensity peak associated with a different mode, m_h, that emerges at small currents and disappears at larger currents, followed by an abrupt onset of a high-intensity spectral peak at a significantly lower frequency that closely matches the auto-oscillation frequency at 295 K [Fig. 3]. The frequency of the mode m_h is somewhat below $f_{\rm FMR}$, and exhibits an approximately linear redshift with increasing current. The two modes do not coexist under any experimental conditions, suggesting that they are mutually exclusive. Furthermore, the transition between the two modes occurs at current $I_{\rm th}$, which decreases with increasing out-of-plane field [Fig. 4(i)], suggesting that the mode m_h is destabilized by the out-of-plane field. Indeed, the current range of the mode m_h shrinks with increasing field, and it is no longer observed at $H \geq 1200$ Oe [Fig. 4(d)].

The field-dependent and current-dependent microwave-generation characteristics discussed above suggest that the high-frequency mode m_h is a localized bullet commonly observed in STNOs [27,36] and SHNOs [13,15,18] with in-plane magnetization. In contract to the bullet mode m_h, the low-frequency mode m_l is characterized by a well-defined threshold current $I_{\rm th}$, above which the intensity abruptly increases, indicating the existence of a barrier for the formation of this mode, as expected for the droplet mode. Similarly to the magnetic droplets in NC STNOs with PMA and an out-of-plane field [33], the frequency of the droplet mode m_l is almost independent of current, except for a weak blueshift close to $I_{\rm th}$ [Fig. 4(f)]. This behavior can be contrasted with that of the bullet mode, which experiences a redshift with increasing current [14,18]. We also note that the spectra obtained at fields $H \leq 960$ Oe exhibit the second harmonic of the mode m_l, consistent with the large amplitude of the magnetization dynamics expected for the droplet mode.

The power-density plots for fields $H = 620$, 800, and 960 Oe [Figs. 4(a)–4(c)] show that the linewidth of the droplet mode m_l is very broad close to its onset, as confirmed by the dependence of the FWHM on current in Fig. 4(g). These behaviors are likely related to the drift instability due to the asymmetry of the effective field and/or the spatial inhomogeneity of the magnetic energy landscape associated with the local variations of PMA in the Co/Ni layer, and are consistent with the existence of an energy barrier for the droplet nucleation [38–40]. At higher currents, the power rapidly increases, while the linewidth decreases, consistent with the theory of nonlinear oscillators [41,42]. Figure 4(h) shows that the integral microwave-generation intensity decreases with increasing

out-of-plane field $H > 960$ Oe, suggesting that the size of the precessing region and/or the amplitude of dynamics decreases with increasing field, consistent with previous studies of the droplet mode [15,38,43]. The minimum FWHM and the integral intensity P_{int} of spectra obtained at the current I_p corresponding to the highest peak PSD [Figs. 4(j) and 4(k)] are largest at small fields, with the largest FWHM of 11 MHz observed at $H = 800$ Oe. The linewidth broadening at small fields is likely associated with the phase noise due to the inhomogeneous distribution of the effective field (including the local variations of magnetic anisotropy and current-induced Oersted fields) coupled with the droplet drift instabilities [38–40,43–45].

C. Temperature dependence of spectral linewidth

We now address the thermal effects on the spectral coherence of the generated microwave signals, and their relation to the dynamical mode structure of the VNC SHNO. Previous theoretical and experimental studies of STNOs showed that, because of the nonlinearity, fluctuations of oscillation amplitude can couple to the phase noise, dramatically reducing the oscillation coherence. These effects are particularly significant close to the transitions between different dynamical modes, where the nonlinearity can become very large, often causing a complex temperature dependence of the linewidth [46–49]. To avoid these anomalous contributions, we analyze the behaviors at current corresponding to the minimum value of the linewidth, at the selected magnetic field and temperature, where such anomalous effects are expected to be small. Figure 5 shows that the minimum linewidth of the low-frequency mode m_l follows a linear dependence on temperature, as illustrated for two large fields. This dependence is consistent with the nonlinear theory of thermal broadening [50] and the thermal-noise model [51] for a single-mode auto-oscillator, as previously shown for a NC STNO and magnetic vortex oscillators [52,53]. The single-mode nature of the magnetization dynamics is confirmed by the Lorentzian line shape of the spectra [Fig. 2(a)]. These behaviors can be contrasted with the thermal effects in the planar-nanogap permalloy/Pt-based SHNO, where the linewidth increases exponentially with temperature, due to the presence of a secondary dynamical mode, and the spectral lines exhibit significant deviations from the Lorentzian shapes [14].

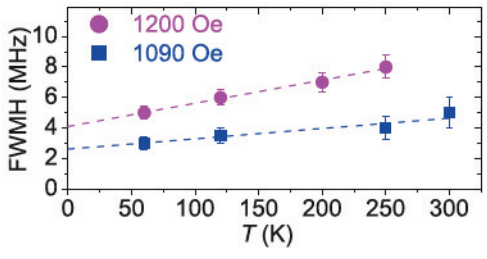

FIG. 5. Minimum linewidth versus T for $H = 1090$ Oe (squares) and $H = 1200$ Oe (circles). The dashed lines are linear fits to the data.

IV. MICROMAGNETIC SIMULATIONS OF AUTO-OSCILLATION

To obtain more insight into the experimentally observed dynamical state in the VNC-SHNO geometry, we perform micromagnetic simulations using OOMMF [54] for a circular Co/Ni disk with a diameter of 1 μm divided into $5 \times 5 \times 1$ nm^3 cells. The simulation includes the effects of spin torque produced by the spin current and the effects of the Oersted field, both calculated with the COMSOL MULTIPHYSICS simulations illustrated in Fig. 1. However, the effects of finite temperature and magnetic inhomogeneities or defects are ignored. The material parameters used in the simulations are as follows: saturation magnetization $M_s = 560$ kA/m, anisotropy constant $K_u = 0.6 \times 10^5$ J/m^3, Gilbert damping constant $\alpha = 0.03$, spin Hall efficiency $P = 0.05$, and exchange stiffness $A = 10$ pJ/m. These parameters are reasonable and are consistent with the values estimated from the FMR measurements of the films studied [28], as well as previously reported values for similar systems. In addition, to avoid parasitic effects of spin-wave reflections from the boundary of the simulated disk [shown by circles in Figs. 6(b) and 6(c)], whose diameter of 1 μm is much smaller than that in our experiments, a highly absorbing boundary is used with damping constant $\alpha = 1$. Figure 6(a) shows a representative calculated auto-oscillation spectrum obtained by micromagnetic simulations at current $I = 14$ mA and out-of-plane magnetic field $H = 1000$ Oe tilted by angle $\varphi = 85°$ relative to the film plane, values similar those used in some of the measurements discussed above. The spectrum is consistent with single-mode oscillation characterized by the fundamental harmonic at frequency $f \sim 1.24$ GHz, and the second harmonic at 2.48 GHz. The oscillation frequencies are in reasonable agreement with the experimental observations discussed above. To gain more insight into how spin current due to the SHE in the Pt layer drives the magnetization auto-oscillation in the VNC SHNO, we also calculate the normalized spatial power maps of the observed dynamical mode, obtained from the time dependence of the local magnetization component m_x^2 [Fig. 6(b)] and m_z^2 [Fig. 6(c)] by our performing pointwise temporal FFT over the simulated area of the Co/Ni disk. Figures 6(b) and 6(c) show that the dynamical mode exhibits an asymmetric elongated spatial profile, with the direction of elongation nearly perpendicular to the in-plane component $H_{\text{in-plane}}$ of the applied magnetic field, and the largest power density localized close to the edge of the nanocontact corresponding to the maximum amplitude of current density. These results confirm that localized standing spin waves

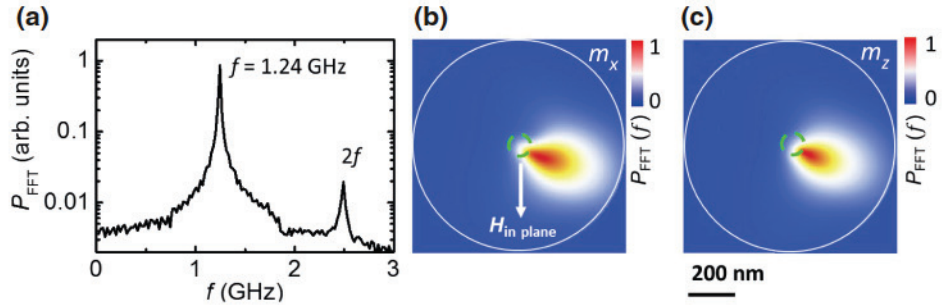

FIG. 6. Micromagnetic simulation of the VNC SHNO. (a) Representative calculated auto-oscillation spectrum showing a single oscillating mode and its second harmonic obtained by micromagnetic simulation at $H = 1000$ Oe applied at angle $\varphi = 85°$ relative to the plane and $I = 14$ mA. (b),(c) Normalized spatial maps of the square of the simulated dynamical magnetization component m_x^2 and m_z^2 of the fundamental mode at $f = 1.24$ GHz. The large solid circle represents the boundary of the active simulation region, the dotted circle marks the nanocontact, and the arrow shows the direction of the in-plane component of the applied oblique field.

can be excited by spin current due to the SHE in the VNC SHNO geometry, and that their spatial characteristics can be efficiently controlled by the in-plane components of the applied and Oersted fields. This conclusion is consistent with the findings of previous theoretical studies of spin-wave excitation due to spin-accumulation-induced spin torque in a single-layer spin-torque nanocontact [55]. One can also expect that broken-symmetry magnetic configurations, involving spin torques arising from the SHE and the interfacial Rashba effect, interfacial Dzyaloshinskii-Moriya interaction, and interfacial PMA, can facilitate other stable dynamical states that can be achieved by varying the material and device parameters. These possibilities warrant further experimental studies, theoretical analysis and numerical modeling of the VNC SHNO geometry presented here.

V. SUMMARY

We demonstrate a spin Hall nano-oscillator formed by a vertical nanocontact fabricated on a Pt/(Co/Ni) bilayer. Several distinct dynamical features are observed when the field, current, and temperature are varied. At cryogenic temperatures, two distinct localized spin-wave modes are observed; a high-frequency mode at small currents and a much-lower-frequency mode at large currents. The former exhibits a nonlinear redshift with increasing current, and is suppressed by the large out-of-plane field, allowing us to identify this mode as the localized bullet mode commonly observed in magnetic nano-oscillators with in-plane magnetization. The low-frequency mode exhibits an almost-negligible nonlinearity, exhibits an abrupt onset, and becomes increasingly stable with increasing out-of-plane magnetic field in the moderate-field range. This mode is identified as the dissipative magnetic droplet stabilized by the local spin current, similar to that previously observed in spin-torque nanocontact nano-oscillators based on magnetic multilayers with PMA. A linear temperature dependence of the minimum linewidth, observed in our VNC SHNO, indicates coherent single-mode auto-oscillation with thermal broadening dominated by intrinsic thermal noise, enabling us to achieve a small linewidth of 4.5 MHz at room temperature. Our results further expand the geometric flexibility of spin Hall oscillators, which may facilitate their applications in spin-wave-based electronic (magnonic) devices and spin-reservoir neuromorphic computing.

ACKNOWLEDGMENTS

L.C., Y.W.D., and R.H.L. are supported by the National Key Research and Development Program of China (Grant No. 2016YFA0300803), the National Natural Science Foundation of China (Grant No. 11774150), the Applied Basic Research Programs of Science and Technology Commission Foundation of Jiangsu Province (Grant No. BK20170627), the Shenzhen Basic Research Program (Grant No. JCYJ20170818110402776), and the Open Research Fund of Jiangsu Provincial Key Laboratory for Nanotechnology. S.U. acknowledges support from the National Science Foundation (Grants No. ECCS-1804198 and No. DMR-1504449).

[1] J. C. Slonczewski, Current-driven excitation of magnetic multilayers, J. Magn. Magn. Mater. **159**, L1 (1996).
[2] L. Berger, Emission of spin waves by a magnetic multilayer traversed by a current, Phys. Rev. B **54**, 9353 (1996).
[3] D. C. Ralph and M. D. Stiles, Spin transfer torques, J. Magn. Magn. Mater. **320**, 1190 (2008).
[4] T. Chen, R. K. Dumas, A. Eklund, P. K. Muduli, A. Houshang, A. A. Awad, P. Dürrenfeld, B. G. Malm, A. Rusu, and J. Åkerman, Spin-torque and spin-Hall nano-oscillators, Proc. IEEE **104**, 1919 (2016).
[5] V. E. Demidov, S. Urazhdin, G. de Loubens, O. Klein, V. Cros, A. Anane, and S. O. Demokritov, Magnetization oscillations and waves driven by pure spin currents, Phys. Rep. **673**, 1 (2017).

[6] V. E. Demidov, S. Urazhdin, and S. O. Demokritov, Direct observation and mapping of spin waves emitted by spin-torque nano-oscillators, Nat. Mater. **9**, 984 (2010).

[7] M. Madami, S. Bonetti, G. Consolo, S. Tacchi, G. Carlotti, G. Gubbiotti, F. B. Mancoff, M. A. Yar, and J. Åkerman, Direct observation of a propagating spin wave induced by spin-transfer torque, Nat. Nanotechnol. **6**, 635 (2011).

[8] H. Ulrichs, V. E. Demidov, S. O. Demokritov, and S. Urazhdin, Spin-torque nano-emitters for magnonic applications, Appl. Phys. Lett. **100**, 162406 (2012).

[9] K. Ando, S. Takahashi, K. Harii, K. Sasage, J. Ieda, S. Maekawa, and E. Saitoh, Electric Manipulation of Spin Relaxation Using the Spin Hall Effect, Phys. Rev. Lett. **101**, 036601 (2008).

[10] L. Q. Liu, C. F. Pai, Y. Li, H. W. Tseng, D. C. Ralph, and R. A. Buhrman, spin-torque switching with the giant Spin Hall effect of tantalum, Science **336**, 555 (2012).

[11] A. R. Mellnik, J. S. Lee, A. Richardella, J. L. Grab, P. J. Mintun, M. H. Fischer, A. Vaezi, A. Manchon, E.-A. Kim, N. Samarth, and D. C. Ralph, Spin transfer torque generated by a topological insulator, Nature **511**, 449 (2014).

[12] W. Han, Y. Otani, and S. Maekawa, Quantum materials for spin and charge conversion, npj Quantum Mater. **3**, 27 (2018).

[13] V. E. Demidov, S. Urazhdin, H. Ulrichs, V. Tiberkevich, A. Slavin, D. Baither, G. Schmitz, and S. O. Demokritov, Magnetic nano-oscillator driven by pure spin current, Nat. Mater. **11**, 1028 (2012).

[14] R. H. Liu, W. L. Lim, and S. Urazhdin, Spectral Characteristics of the Microwave Emission by the Spin Hall Nano-Oscillator, Phys. Rev. Lett. **110**, 147601 (2013).

[15] R. H. Liu, W. L. Lim, and S. Urazhdin, Dynamical Skyrmion State in a Spin Current Nano-Oscillator with Perpendicular Magnetic Anisotropy, Phys. Rev. Lett. **114**, 137201 (2015).

[16] M. Ranjbar, P. Dürrenfeld, M. Haidar, E. Iacocca, M. Balinskiy, T. Q. Le, M. Fazlali, A. Houshang, A. Awad, R. K. Dumas, and J. Åkerman, CoFeB based spin Hall nano-oscillators, IEEE Magn. Lett. **5**, 3000504 (2014).

[17] R. H. Liu, L. Chen, S. Urazhdin, and Y. W. Du, Controlling the Spectral Characteristics of a Spin-Current Auto-Oscillator with an Electric Field, Phys. Rev. Appl. **8**, 021001 (2017).

[18] L. Chen, K. Zhou, S. Urazhdin, W. Jiang, Y. W. Du, and R. H. Liu, Dynamical mode coexistence and chaos in the nano-gap spin Hall nano-oscillator, Phys. Rev. B **100**, 104436 (2019).

[19] L. Chen, S. Urazhdin, Y. W. Du, and R. H. Liu, Dynamical Mode Coupling and Coherence in a Spin Hall Nano-Oscillator with Perpendicular Magnetic Anisotropy, Phys. Rev. Appl. **11**, 064038 (2019).

[20] H. Ulrichs, V. E. Demidov, and S. O. Demokritov, Micromagnetic study of auto-oscillation modes in spin-Hall nano-oscillators, Appl. Phys. Lett. **104**, 042407 (2014).

[21] Z. Duan, A. Smith, L. Yang, B. Youngblood, J. Lindner, V. E. Demidov, S. O. Demokritov, and I. N. Krivorotov, Nanowire spin torque oscillator driven by spin orbit torques, Nat. Commun. **5**, 1038 (2014).

[22] A. Zholud and S. Urazhdin, Microwave generation by spin Hall nanooscillators with nanopatterned spin injector, Appl. Phys. Lett. **105**, 112404 (2014).

[23] V. E. Demidov, S. Urazhdin, A. Zholud, A. V. Sadovnikov, and S. O. Demokritov, Nanoconstriction-based spin-Hall nano-oscillator, Appl. Phys. Lett. **105**, 172410 (2014).

[24] H. Mazraati, S. Chung, A. Houshang, M. Dvornik, L. Piazza, F. Qejvanaj, S. Jiang, T. Q. Le, J. Weissenrieder, and J. Åkerman, Low operational current spin Hall nano-oscillators based on NiFe/W bilayers, Appl. Phys. Lett. **109**, 242402 (2016).

[25] H. Mazraati, S. R. Etesami, S. A. H. Banuazizi, S. Chung, A. Houshang, A. A. Awad, M. Dvornik, and J. Åkerman, Auto-oscillating Spin-Wave Modes of Constriction-Based Spin Hall Nano-oscillators in Weak In-Plane Fields, Phys. Rev. Appl. **10**, 054017 (2018).

[26] G. H. O. Daalderop, P. J. Kelly, and F. J. A. den Broeder, Prediction and Confirmation of Perpendicular Magnetic Anisotropy in Co/Ni Multilayers, Phys. Rev. Lett. **68**, 682 (1992).

[27] A. Slavin and V. Tiberkevich, Spin Wave Mode Excited by Spin-Polarized Current in a Magnetic Nanocontact is a Standing Self-Localized Wave Bullet, Phys. Rev. Lett. **95**, 237201 (2005).

[28] See Supplemental Materialat http://link.aps.org/supplemental/10.1103/PhysRevApplied.13.024034 for the magnetic properties of Pt/(Co/Ni) multilayer films.

[29] A. Al Subhi and R. Sbiaa, Control of magnetization reversal and domain structure in (Co/Ni) multilayers, J. Magn. Magn. Mater. **489**, 165460 (2019).

[30] COMSOL Multiphysics, COMSOL Multiphysics, COMSOL AB, Stockholm, Sweden. www.comsol.com.

[31] J. C. Sankey, P. M. Braganca, A. G. F. Garcia, I. N. Krivorotov, R. A. Buhrman, and D. C. Ralph, Spin-Transfer-Driven Ferromagnetic Resonance of Individual Nanomagnets, Phys. Rev. Lett. **96**, 227601 (2006).

[32] W. H. Rippard, A. M. Deac, M. R. Pufall, J. M. Shaw, M. W. Keller, S. E. Russek, G. E. W. Bauer, and C. Serpico, Spin-transfer dynamics in spin valves with out-of-plane magnetized CoNi free layers, Phys. Rev. B **81**, 014426 (2010).

[33] S. M. Mohseni, S. R. Sani, J. Persson, T. N. A. Nguyen, S. Chung, Y. Pogoryelov, P. K. Muduli, E. Iacocca, A. Eklund, R. K. Dumas, S. Bonetti, A. Deac, M. A. Hoefer, and J. Åkerman, Spin torque-generated magnetic droplet solitons, Science **339**, 1295 (2013).

[34] F. Macià, D. Backes, and A. D. Kent, Stable magnetic droplet solitons in spin-transfer nanocontacts, Nat. Nanotechnol. **9**, 992 (2014).

[35] M. A. Hoefer, T. J. Silva, and M. W. Keller, Theory for a dissipative droplet soliton excited by a spin torque nanocontact, Phys. Rev. B **82**, 054432 (2010).

[36] S. Bonetti, V. Tiberkevich, G. Consolo, G. Finocchio, P. Muduli, F. Mancoff, A. Slavin, and J. Åkerman, Experimental Evidence of Self-Localized and Propagating Spin Wave Modes in Obliquely Magnetized Current-Driven Nanocontacts, Phys. Rev. Lett. **105**, 217204 (2010).

[37] S. Lendínez, J. Hang, S. Vélez, J. M. Hernàndez, D. Backes, A. D. Kent, and F. Macià, Effect of Temperature on Magnetic Solitons Induced by Spin-transfer Torque, Phys. Rev. Appl. **7**, 054027 (2017).

[38] N. Statuto, C. Hahn, J. M. Hernàndez, A. D. Kent, and F. Macià, Multiple magnetic droplet soliton modes, Phys. Rev. B **99**, 174436 (2019).

[39] S. Lendínez, N. Statuto, D. Backes, A. D. Kent, and F. Macià, Observation of droplet soliton drift resonances in a spin-transfer-torque nanocontact to a ferromagnetic thin film, Phys. Rev. B **92**, 174426 (2015).

[40] P. Wills, E. Iacocca, and M. A. Hoefer, Deterministic drift instability and stochastic thermal perturbations of magnetic dissipative droplet solitons, Phys. Rev. B **93**, 144408 (2016).

[41] J. V. Kim, V. Tiberkevich, and A. N. Slavin, Generation Linewidth of an Auto-oscillator with a Nonlinear Frequency Shift: Spin-Torque Nano-Oscillator, Phys. Rev. Lett. **100**, 017207 (2008).

[42] A. Slavin and V. Tiberkevich, Nonlinear auto-oscillator theory of microwave generation by spin-polarized current, IEEE Trans. Magn. **45**, 1875 (2009).

[43] B. Divinskiy, S. Urazhdin, V. E. Demidov, A. Kozhanov, A. P. Nosov, A. B. Rinkevich, and S. O. Demokritov, Magnetic droplet solitons generated by pure spin currents, Phys. Rev. B **96**, 224419 (2017).

[44] M. Mohseni, M. Hamdi, H. F. Yazdi, S. A. H. Banuazizi, S. Chung, S. R. Sani, J. Åkerman, and M. Mohseni, Magnetic droplet soliton nucleation in oblique fields, Phys. Rev. B **97**, 184402 (2018).

[45] R. O. Moore and M. A. Hoefer, Stochastic ejection of nanocontact droplet solitons via drift instability, Phys. Rev. B **100**, 014402 (2019).

[46] E. Iacocca, P. Dürrenfeld, O. Heinonen, J. Åkerman, and R. K. Dumas, Mode-coupling mechanisms in nanocontact spin-torque oscillators, Phys. Rev. B **91**, 104405 (2015).

[47] E. Iacocca, O. Heinonen, P. K. Muduli, and J. Åkerman, Theory generation linewidth of mode-hopping spin torque oscillators, Phys. Rev. B **89**, 054402 (2014).

[48] S. S. L. Zhang, E. Iacocca, and O. Heinonen, Theory Tunable Mode Coupling in Nanocontact Spin-torque Oscillators, Phys. Rev. Appl. **8**, 014034 (2017).

[49] P. K. Muduli, O. G. Heinonen, and J. Åkerman, Temperature dependence of linewidth in nanocontact based spin torque oscillators: Effect of multiple oscillatory modes, Phys. Rev. B **86**, 174408 (2012).

[50] V. Tiberkevich, A. Slavin, and J. V. Kim, Temperature dependence of nonlinear auto-oscillator linewidths: Application to spin-torque nano-oscillators, Phys. Rev. B **78**, 092401 (2008).

[51] T. J. Silva and M. W. Keller, Theory of thermally induced phase noise in spin torque oscillators for a high-symmetry case, IEEE Trans. Magn. **46**, 3555 (2010).

[52] P. Bortolotti, A. Dussaux, J. Grollier, V. Cros, A. Fukushima, H. Kubota, K. Yakushiji, S. Yuasa, K. Ando, and A. Fert, Temperature dependence of microwave voltage emission associated to spin-transfer induced vortex oscillation in magnetic tunnel junction, Appl. Phys. Lett. **100**, 042408 (2012).

[53] J. F. Sierra, M. Quinsat, F. Garcia-Sanchez, U. Ebels, I. Joumard, A. S. Jenkins, B. Dieny, M. C. Cyrille, A. Zeltser, and J. A. Katine, Influence of thermal fluctuations on the emission linewidth in mgO-based spin transfer oscillators, Appl. Phys. Lett. **101**, 062407 (2012).

[54] M. J. Donahue and D. G. Porter, OOMMF (NIST), http://math.nist.gov/oommf.

[55] M. Hoefer, T. Silva, and M. Stiles, Model for a collimated spin-wave beam generated by a single-layer spin torque nanocontact, Phys. Rev. B **77**, 144401 (2008).